

Review

# Progress in Synthesizing Analogues of Nitrogenase Metalloclusters for Catalytic Reduction of Nitrogen to Ammonia

Jianjun Yang <sup>1,2</sup>

<sup>1</sup> Department of Chemical Engineering, School of Environmental Science and Engineering, Chang'an University, Xi'an 710064, China; jjyang@chd.edu.cn; Tel.: +86-29-82339051

<sup>2</sup> Key Laboratory of Subsurface Hydrology and Ecological Effects in Arid Region (Chang'an University), Ministry of Education, Xi'an 710064, China

Received: 17 October 2019; Accepted: 4 November 2019; Published: 8 November 2019



**Abstract:** Ammonia (NH<sub>3</sub>) has played an essential role in meeting the increasing demand for food and the worldwide need for nitrogen (N<sub>2</sub>) fertilizer since 1913. Unfortunately, the traditional Haber-Bosch process for producing NH<sub>3</sub> from N<sub>2</sub> is a high energy-consumption process with approximately 1.9 metric tons of fossil CO<sub>2</sub> being released per metric ton of NH<sub>3</sub> produced. As a very challenging target, any ideal NH<sub>3</sub> production process reducing fossil energy consumption and environmental pollution would be welcomed. Catalytic NH<sub>3</sub> synthesis is an attractive and promising alternative approach. Therefore, developing efficient catalysts for synthesizing NH<sub>3</sub> from N<sub>2</sub> under ambient conditions would create a significant opportunity to directly provide nitrogenous fertilizers in agricultural fields as needed in a distributed manner. In this paper, the literature on alternative, available, and sustainable NH<sub>3</sub> production processes in terms of the scientific aspects of the spatial structures of nitrogenase metalloclusters, the mechanism of reducing N<sub>2</sub> to NH<sub>3</sub> catalyzed by nitrogenase, the synthetic analogues of nitrogenase metalloclusters, and the opportunities for continued research are reviewed.

**Keywords:** ammonia synthesis; FeMo-cofactor; nitrogenase metallocluster; analogue; nitrogen

## 1. Introduction

As one of the most important chemicals on our planet, NH<sub>3</sub> has met the growing demand for food and worldwide nitrogen fertilizer since 1913 [1]. Total worldwide NH<sub>3</sub> production exceeded 140 million tons in 2014 and continues to grow [2], and approximately 80% of the NH<sub>3</sub> produced is used as nitrogen fertilizer. Fritz Haber discovered that NH<sub>3</sub> could be directly synthesized by reacting atmospheric N<sub>2</sub> with hydrogen in the temperature range of 400–500 °C and at pressures of 130–170 bar [3], and Carl Bosch subsequently developed it on an industrial scale [4]. As the so-called most important invention of the 20th century, the Haber-Bosch process, a thermo-chemical catalytic conversion technology, is still the primary choice for industrial production of NH<sub>3</sub>. According to the Haber-Bosch process, NH<sub>3</sub> is produced from the reaction:



Having been optimized in large industrial facilities over many years [5], the process has significantly benefited humans including feeding the world's growing population via the use of nitrogen fertilizer. However, the overuse of N<sub>2</sub> fertilization has become a problematic issue, as excess fixed N<sub>2</sub> affects ecosystem balance, human health, and climate change accounting for 1% of global greenhouse gas

emissions. More than 1.9 metric tons of fossil carbon dioxide is released per metric ton of  $\text{NH}_3$  produced in the best-case scenario of using natural gas to obtain hydrogen,  $\text{N}_2$ , and energy [2]. The distribution of fertilizer produced by the Haber-Bosch process requires efficient transportation that may be more difficult in developing countries than in developed countries. From saturated fertilizers, the loss of over 40% of reactive  $\text{N}_2$  causes algae growth in natural waters and unbalances ecosystems near farms [6] causing significant  $\text{N}_2$  pollution of the soil [7].

The Haber-Bosch process reacts the pure feed gases at high temperatures and pressures, requiring an energy input of approximately  $485 \text{ kJ mol}^{-1}$  of  $\text{N}_2$  and almost 2% of global energy consumption [8]. Therefore, any  $\text{NH}_3$  production process that can reduce fossil energy consumption and environmental pollution would be welcomed. Actually, the high dissociation energy of the triple-bonded  $\text{N}_2$  molecule ( $911 \text{ kJ mol}^{-1}$ ) presents a significant activation energy barrier; however, the negative enthalpy ( $\Delta H_{300} = -46.35 \text{ kJ mol}^{-1}$ ) of the reaction dictates that  $\text{N}_2$  could be converted to  $\text{NH}_3$  at lower temperatures [9]. Thus, finding a solution that activates the  $\text{N}\equiv\text{N}$  bond to produce  $\text{NH}_3$  with less fossil energy consumption is a great opportunity and challenge for chemists. Artificial catalysts should be able to facilitate the reaction at moderate conditions. Although there are many new approaches, the industrial catalysts used today are extremely similar to the initial catalysts discovered by Mittasch in the 1910 s [10]. The use of energy from sustainable sources, such as solar, in an alternative sustainable  $\text{NH}_3$  synthesis process based on the biological fixation of  $\text{N}_2$  would be more energy efficient than the Haber-Bosch process [11]. In addition, it would be possible to produce nitrogen fertilizers close to agricultural farms as needed and reduce greenhouse gas emissions and control the global  $\text{N}_2$  cycle. Therefore, developing efficient catalysts for synthesizing  $\text{NH}_3$  from  $\text{N}_2$  under ambient conditions could directly provide nitrogenous fertilizers in agricultural fields as needed in a distributed manner, creating significant opportunities.

There are several advantages for  $\text{NH}_3$  synthesis at ambient temperatures [12,13]. Firstly, the reaction from producing  $\text{NH}_3$  from  $\text{N}_2$  with hydrogen is spontaneous. Secondly, the proton conductivity of low-temperature electrolytes performs better than the higher temperature electrolytes. Thirdly, the reaction kinetics of the  $\text{NH}_3$  production processes are extremely slow when operating temperatures are below  $100 \text{ }^\circ\text{C}$ . In addition, it would be a key point around which to build the foundational principles of designing new efficient catalysts for a sustainable  $\text{NH}_3$  synthesis production process. Obviously, due to the fact of its energy savings and environmental friendliness, biological  $\text{N}_2$  fixation would be an excellent alternative to the Haber-Bosch process. Until now, nitrogenase was the only known enzyme capable of catalytic reduction of  $\text{N}_2$  to  $\text{NH}_3$  under moderate conditions. Over the past five decades, researchers have taken inspiration from nitrogenase metal clusters and have focused their efforts on synthesizing either analogues or the unique topology of the catalytic activity cores of nitrogenase, and their functional principles have been applied in building novel catalysts for synthesizing  $\text{NH}_3$  from  $\text{N}_2$  at ambient temperatures and pressures. There are some advantages of synthetic metallocluster analogues over nitrogenase for the reduction of  $\text{N}_2$  to  $\text{NH}_3$ : (1) Compared with natural nitrogenase (protein), the synthetic analogues, which have very stable molecular structures, are less likely to lose their catalytic activity. (2) The synthetic analogues of nitrogenase metalloclusters in the carriers are easier to recover and reuse than the natural nitrogenase the lowering its application cost. (3) The synthetic analogues, but not nitrogenase, can be redesigned according to need by introducing auxiliary factors to obtain new analogues with stronger catalytic activity.

The new methods of catalyst design require us to understand catalytic mechanisms by integrating theory and experiment thereby discovering active, scalable, selective, and long-lived efficient catalysts for sustainable  $\text{NH}_3$  synthesis. Based on the detailed insights into the nitrogenase reaction mechanism, by mimicking its reactive centers, synthesizing the analogues of metalloclusters in nitrogenase, and investigating the complex assembly pathways, an opportunity to develop novel efficient catalysts for sustainable  $\text{NH}_3$  synthesis should be provided [14]. In this paper, the literature on alternative, available, and sustainable  $\text{NH}_3$  production processes in respect to the spatial structures of nitrogenase

metalloclusters, the mechanism that reduces  $N_2$  to  $NH_3$  catalyzed by nitrogenase, and the synthetic analogues of metalloclusters in nitrogenase are reviewed.

## 2. Nitrogenase Metalloclusters

Nitrogenases (EC 1.18.6.1, EC 1.19.6.1) are produced by bacteria including Cyanobacteria, green sulfur bacteria, *Azotobacter*, *Rhizobium*, and *Spirillum*. It is understandable that there are many different structures and mechanisms across the numerous nitrogenase variants, as their biochemical processes evolved in completely different and diverse organisms for two thousand million years [15]. It is well known that only nitrogenase can catalyze the reduction of  $N_2$  to  $NH_3$  at relatively high rates (turnover frequency, TOF  $\approx 2 NH_3 s^{-1}$ ) with relatively high turnover numbers (TON  $> 10^6$ ) at room temperature and atmospheric pressure [16] in order to maintain the biogeochemical  $N_2$  cycle and sustain life on Earth. There is an overall negative enthalpy of reaction ( $\Delta H^0 = -45.2 KJ mol^{-1} NH_3$ ) and high activation energy ( $E_a = 230-420 KJ mol^{-1}$ ) in the equilibrium formation of  $NH_3$  from molecular hydrogen and  $N_2$  [17]. Therefore, the reduction of  $N_2$  to  $NH_3$  can take place in the presence of nitrogenase as a catalyst by reducing this reaction energy barrier at room temperature and atmospheric pressure; this is a key driving force in the development of efficient catalytic  $N_2$  fixation processes.

Over the past five decades, much progress has been made in the fundamental understanding of nitrogenase and the mechanism by which it catalyzes  $N_2$  to  $NH_3$  as well as in identifying significant intermediates [18]. Nitrogenase consists of two proteins: ferritin(Fe)-protein and molybdenum (Mo)-ferritin protein which are called Fe-protein and MoFe-protein, respectively. The Fe-protein consists of two MgATP binding sites and an [4Fe4S] cluster. It weighs approximately 64 KDa [19]. The Fe-protein is an  $\alpha_2$  homodimer consisting of two subunit proteins that bind to the [4Fe4S] cluster [15]. As for the main protein, there is a FeMo-cofactor (FeMo-co, [MoFe<sub>7</sub>S<sub>9</sub>X], X=C, N, or O) and a P-cluster [Fe<sub>8</sub>S<sub>7</sub>] [20].

## 3. Reduction Mechanism of $N_2$ to $NH_3$

Nitrogenase is the only known biological system that has the capability of reducing atmospheric  $N_2$  to  $NH_3$  [21]. The Fe-proteins and the MoFe-proteins of nitrogenase together catalyze the reduction of  $N_2$  to  $NH_3$  with an ideal reaction stoichiometry [22]:



The mechanism of reducing  $N_2$  to  $NH_3$  by nitrogenase is shown in Figure 1. As a homodimer with two nucleotide (magnesium-adenosine-triphosphate, termed MgATP, or magnesium-adenosine-diphosphate, termed MgADP) binding sites; the Fe-protein has a single [4Fe4S] cluster that bridges its two subunits, one of which has one binding site [19] that is the only known reductant of the MoFe-protein. The Fe-protein has a high reducing power and is responsible for the supply of electrons in the reduction process of  $N_2$  to  $NH_3$  [23]. The MoFe-protein contains two catalytic units: the P-cluster and the FeMo-co. The P-cluster is placed between the Fe-protein [4Fe4S] cluster and the FeMo-co by two different stable Fe-protein-MoFe-protein complexes as shown in Figure 1. The P-clusters are believed to mediate the electron transfer between the Fe-protein and the substrate reduction site of the FeMo-co [24,25]. The transient complex allows the reductive equivalents to be passed to the MoFe-protein, and the electron transfer is coupled to the hydrolysis of MgATP [15,16]. One electron is transferred and two equivalents of MgATP are hydrolyzed for each encounter complex. Actually, the reduction of  $N_2$  is activated by the electrons which are delivered from either ferredoxins or flavodoxins to the MoFe-protein, where the catalytic process is mediated by way of the Fe-protein [16]. The formation of the Fe-protein and MoFe-protein complex is beneficial to the intermolecular electrons' transfer which is driven by the MgATP hydrolysis and will dissociate to restart and accumulate the necessary electrons needed for  $N_2$  reduction when the hydrolysis and the transfer are complete [26,27]. Moreover, through the associated Fe-protein conformational changes, a stepwise mechanism is anticipated to prolong the lifetime

of the Fe-protein–MoFe-protein complex which, in turn, could orchestrate the sequence of intra-complex electron-transfer required for substrate reduction [28].

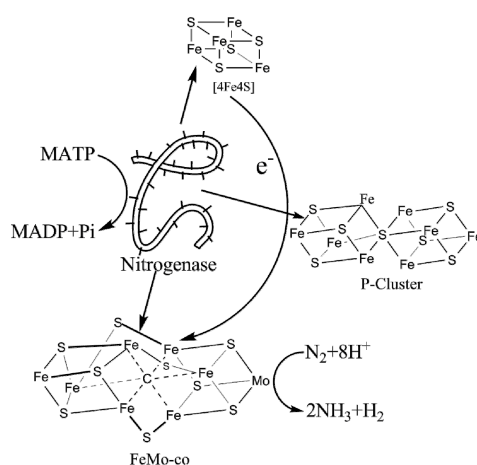


**Figure 1.** The [4Fe4S] cluster, P-cluster, FeMo-co, and electron transfer pathway. For electron transfer, the P-cluster plays an important role in bridging the Fe–S cluster and the FeMo-co embedded in the a-subunit of the MoFe-protein [29]. The FeMo-co uses the electrons provided by the P-cluster to reduce  $N_2$  to  $NH_3$  [11]. The FeMo-co are usually the site of substrate binding and reduction. That is to say, the MoFe-protein alone will not reduce  $N_2$  in the absence of the electron transfer step of the Fe-protein.

The Lowe and Thorneley (LT) [30] kinetic model involves eight steps which are needed. This involves only adding six hydrogen atoms to the  $N_2$  for the formation of  $NH_3$ , because  $H_2$  is released in the process. As shown in Figure 2, when the MoFe-proteins sequentially gain more electrons, they become more reducing, denoted by “E”, and their resting state is  $E_0$ . With the gain in electrons from the Fe-protein, E goes through conformational changes. The dissociation of the MgADP from the Fe-protein after transferring electrons to the P-cluster is the rate limiting step [31].

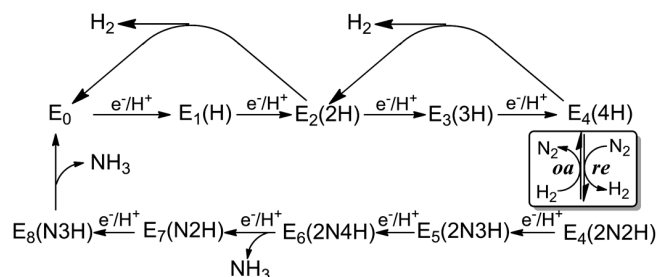


**Figure 2.** Lowe-Thorneley kinetic model for the reduction of  $N_2$  to  $NH_3$  catalyzed by nitrogenase [21].

The mechanism mainly describes the accumulation of multiple electrons and protons at the active site of FeMo-co before  $N_2$  can bind, and the loss of electrons and protons through the formation of hydrogen has been well accepted by researchers who have tried to demonstrate the relationship between intermediates and specific states of the LT model by capturing and characterizing different intermediates [15]. Although it is challenging because these captured states may not match the specific states of this model, these captured and characterized states are helpful for completely understanding the nitrogenase catalyzed reduction pathway of  $N_2$  to  $NH_3$  with molecular level insight. In the present study, two hydrides should leave to allow  $N_2$  activation in the  $E_4$  step. After rotating one proton from FeMo-co to release one of the bonds to Mo,  $N_2$  can bind. The  $N_2$  protonation steps are energetically easy [32]. Generally speaking, enzymatic reduction of  $N_2$  to  $NH_3$  by nitrogenase seemly follows the LT kinetics model. Researchers are relatively confident regarding the structures of the first four intermediates ( $E_0$ – $E_4$ ) and, for a while, some believed an alternating pathway might be followed for subsequent  $N_2$  reduction.

In addition to FeMo-co, Kaczmarek et al. [33] developed a biomimetic mononuclear iron model for the catalytic reduction of  $N_2$  to  $NH_3$  using catalyst  $(TPB)FeN_2$  (tris(phosphine)borate) complex with a biomimetic mononuclear iron center. They found that the lowest energy pathway among several possible  $NH_3$  formation pathways in a natural environment is the consecutive addition of three protons to the same site which has implications for nitrogenases. Coincidentally, the homogeneous  $N_2$  reduction to  $NH_3$  may be catalyzed by artificial nitrogenases  $EP_3Fe^-N_2^-$  ( $E = B, Si$ ) as single site iron complexes. It was found that the catalytic mechanism depends on the applied ligand, and that the energy pathway using catalyst  $BP_3Fe^-N_2^-$  is the most favorable route with descending Gibbs free energy [34]. Currently, more studies are being carried out either prove or disprove the recent literature or to provide answers to the problems they raise.

#### 4. Synthesizing Analogues of Nitrogenase Metalloclusters

The discovery of the three unprecedented metalloclusters has led to synthesized analogues of these clusters for  $NH_3$  biosynthesis [35]. As precursors, the  $[4Fe4S]$  clusters could provide a higher nuclearity P-cluster and FeMo-co in the Fe-protein component and MoFe-proteins of nitrogenase [36]. Researchers should consider the details of the synthetic analogue methods. For example, the amino acid side chains of the nitrogenase molecule may be necessary to maintain the P-cluster structure. Functionally, the faithfully synthesized analogs of these clusters must be coordinated with each other to reduce  $N_2$  to  $NH_3$ . However, the synthesized clusters are not very close to the biological clusters in terms of spatial structure, spectral characteristics, and catalytic function. Therefore, these clusters are challenging synthetic targets because of their intriguing and unprecedented features.

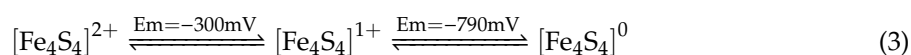
Although synthetic analogues of nitrogenase metalloclusters are promising artificial catalytic clusters due to the fact of their intriguing features, no synthesized clusters have been constructed completely similar to the biogenic clusters, especially in the catalytic functional and capacity aspects [35]. Synthesizing analogues of the nitrogenase active site is an important approach to elucidate the properties of these metal-sulfur clusters and is a major challenge for chemists in developing sustainable  $NH_3$  synthesis processes under ambient conditions. From the structural and mechanistic reduction of  $N_2$  to  $NH_3$  standpoints, accurately synthesizing analogue clusters that can activate the strong bond of  $N_2$  at ambient conditions is an important step toward accomplishing this kind of catalyst design [23].

##### 4.1. Synthesizing Analogues of $[4Fe4S]$ Clusters

###### 4.1.1. Structure of $[4Fe4S]$ Clusters

As an integral part of nitrogenase, the Fe-protein provides the MoFe-protein with electrons which are used to break the  $N_2$  triple bond. Among the 20 different nitrogenases studied, 45–90% share similarities in amino acid sequences [37]. However, there is a considerable similarity in the different  $[4Fe4S]$  clusters of different Fe-proteins from different nitrogenases.

In 1994, Watt and Reddy [31] reported that the  $[Fe_4S_4]^+$  state of the Fe-protein could be further reduced using methyl viologen. In the normal resting state of the  $[4Fe4S]$  cluster (Figure 1), it changes to  $[Fe_4S_4]^{2+}$  from  $[Fe_4S_4]^+$  when it donates an electron to the P-cluster [16]. Simultaneously, with the charge changing of the complex, its conformation also changes [38]. Dithionite as a reductant only reduces the oxidized  $[Fe_4S_4]^{2+}$  cluster to  $[Fe_4S_4]^+$  (as shown in Equation (3)). If the  $[4Fe4S]$  cluster could be reduced to  $[Fe_4S_4]^0$ , then the cluster could potentially supply two electrons to the MoFe-protein for breaking the very strong  $N_2$  triple bond. Actually, the  $[4Fe4S]$  cluster has an additional reduced state,  $[Fe_4S_4]^0$ , and  $Ti(III)Cl_3$  as a reductant reducing  $[4Fe4S]$  cluster could supply two electrons to the process [39]. The structure of a non-dissociating nitrogenase complex suggests two electron transfer pathways from the Fe-protein  $[4Fe4S]$  cluster to the MoFe-protein P-cluster [40]. Both the P-cluster and the FeMo-co might be able to accept two electrons, and all substrates of nitrogenase are reduced in multiples of two electrons [16].



#### 4.1.2. Preparation of [4Fe4S] Clusters

The spontaneous assembly of Fe atoms in the presence of sulfur reagents is an efficient and common method for synthesizing [4Fe4S] clusters and synthetic analogues of nitrogenase biological clusters. The properties and reactivity of synthesizing [4Fe4S] clusters found in Fe-proteins are governed by several factors, especially as a ligand and a reductant for  $\text{Fe}^{3+}$ , one of which is excess thiolate ( $-\text{SR}$ ) that forms disulfides in the process.

The early synthetic methods involved ferritin (usually  $\text{FeCl}_2$  or  $\text{FeCl}_3$ ) with thiolates and sulfide sources (e.g.,  $\text{HS}^-$ ,  $\text{S}^{2-}$ ) in polar organic solvents such as methanol and N,N-dimethylformamide (DMF). The halide-terminated clusters with  $\text{X} = \text{Cl}$  and  $\text{Br}$  give irreversible  $[\text{Fe}_4\text{S}_4\text{X}_4]^{3-/4-}$  reductions [41]. Thus, the thiolate species are more difficultly reduced than the halide species, but the reductions give tetra anions that are unstable on the time scale of the experiment. Interestingly, the addition of phosphine irreversibly reduces the halide-terminated  $[\text{Fe}_4\text{S}_4\text{X}_4]^{2-}$  to the  $[\text{Fe}_4\text{S}_4]^+$  level at  $-1.2$  V in the neutral product  $[\text{Fe}_4\text{S}_4(\text{P}^t\text{Bu}_3)_3\text{X}]$  with mixed unstable ligation, and some of the phosphine is oxidized to the phosphine sulfide [42]. With a slight excess of large tertiary phosphines, all four ferritin atoms were possibly substituted to yield  $[\text{Fe}_4\text{S}_4(\text{PR}_3)_4]^+$  ( $\text{R} = \text{Bu}^t$ ,  $\text{Cy}$ ,  $\text{Pri}$ ) [43]. Alternatively,  $[\text{Fe}_4\text{S}_4(\text{PR}_3)_4]^0$  can be prepared by chemical reduction of the mono-cation with a slight excess of sodium acenaphthalenide. These neutral clusters are so sensitive to oxidation that they have stability only for a few days in solution [44] such as the neutral  $[\text{Fe}_4\text{S}_4(\text{PR}_3)_4]$  clusters [43]. It is interesting to understand whether the stability of these  $[\text{Fe}_4\text{S}_4(\text{PR}_4)_4]$  clusters would lead to sulfur-based reactivity with substrates. Metalation with the Fe-S cluster precursor  $[\text{Ph}_4\text{P}]_2[\text{Fe}_4\text{S}_4\text{Cl}_4]$  provides clusters of different nuclearity that may be controlled with high selectivity through simple and rational modification of the steric profiles of the ligands [45].

Usually,  $\text{FeCl}_3$ ,  $\text{RS}^-$  and hydrosulfide can generate a series of [4Fe4S] clusters with the general formula  $[\text{Fe}_4\text{S}_4(\text{SR})_4]^Y$  ( $Y = 0, 1-, 2-, 3-,$  and  $4-$  as shown in Table 1) [46] including the most common class of biomimetic [4Fe4S] clusters,  $[\text{Fe}_4\text{S}_4(\text{SCH}_2\text{Ph})_4]^{2-}$  [47]. On the other hand, for the phenoxide-terminated cluster  $[\text{Fe}_4\text{S}_4(\text{OPh})_4]^{2-}$ , two electrochemically reversible reduction features at  $-1.6$  V [48] are somewhat more cathodic than the thiolate analogues. The [4Fe4S] clusters can also be obtained by means of core conversions among different Fe-S clusters, for example, by using two  $[\text{Fe}_2\text{S}_2]^{2+}$  clusters to form a cubic  $[\text{Fe}_4\text{S}_4]^{2+}$  cluster in aqueous solution and especially by synthesizing  $[\text{Fe}_4\text{S}_4(\text{SEt})_4]^{2-}$  by heating a saturated acetonitrile solution of  $[\text{Fe}_2\text{S}_2(\text{SEt})_4]^{2-}$  up to  $80$  °C [49].  $[\text{Fe}_2\text{S}_2(\text{SPh})_4]^{2-}$  can also be electrochemically reduced to the corresponding  $[\text{Fe}_4\text{S}_4]^{2+}$  cluster [50].

**Table 1.** Core oxidation state of  $[\text{Fe}_4\text{S}_4(\text{SR})_4]^{0/1-/2-/3-/4-}$  analogues [43].

| Analogues                      | $[\text{Fe}_4\text{S}_4(\text{SR})_4]^0$ | $[\text{Fe}_4\text{S}_4(\text{SR})_4]^{1-}$ | $[\text{Fe}_4\text{S}_4(\text{SR})_4]^{2-}$ | $[\text{Fe}_4\text{S}_4(\text{SR})_4]^{3-}$ | $[\text{Fe}_4\text{S}_4(\text{SR})_4]^{4-}$ |
|--------------------------------|--|---|---|---|---|
| Core oxidation state           | $[\text{Fe}_4\text{S}_4]^{4+}$           | $[\text{Fe}_4\text{S}_4]^{3+}$              | $[\text{Fe}_4\text{S}_4]^{2+}$              | $[\text{Fe}_4\text{S}_4]^{1+}$              | $[\text{Fe}_4\text{S}_4]^0$                 |
| Composition of oxidation state | 4Fe(III)                                 | 3Fe(III) + Fe(II)                           | 2Fe(III) + 2Fe(II)                          | Fe(III) + 3Fe(II)                           | 4Fe(II)                                     |

As indicated in Tables 1 and 2, most examples of synthetic  $[\text{Fe}_4\text{S}_4(\text{SR})_4]^{2-}$  clusters in the  $[\text{4Fe4S}]^{2+}$  state have been reported [42]. However, because the  $[\text{Fe}_4\text{S}_4(\text{SR})_4]^0$  cluster in the  $[\text{4Fe4S}]^{4+}$  state and the  $[\text{Fe}_4\text{S}_4(\text{SR})_4]^{4-}$  cluster in the  $[\text{4Fe4S}]^0$  state should be extremely unstable, there are only a few examples of  $[\text{Fe}_4\text{S}_4(\text{SR})_4]^0$  and  $[\text{Fe}_4\text{S}_4(\text{SR})_4]^{4-}$  which still remain elusive [43,51]. In synthesizing analogues of the [4Fe4S] cluster processes using the general formula  $[\text{Fe}_4\text{S}_4(\text{SR})_4]^Y$ , elemental sulfur works not only as the source of the [4Fe4S] core sulfur atoms, but also as an oxidant to induce the reductive elimination of disulfides from thiolate ligands on iron [52].

The spontaneous assembly reactions driven by increasing the number of Fe atoms in a stepwise manner should terminate when the Fe-S cluster products become stable. The dianionic [4Fe4S] cluster  $[\text{Fe}_4\text{S}_4(\text{SR})_4]^{2-}$  with an  $[\text{Fe}_4\text{S}_4]^{2+}$  core is the most thermo-dynamically stable Fe-S cluster. To avoid this

stability, synthesizing Fe–S clusters with more than four Fe atoms can be realized via destabilization of  $[\text{Fe}_4\text{S}_4(\text{SR})_4]^{2-}$  [47] or by changing the oxidation state. The encapsulation of the [4Fe4S] cluster core by bulky substituents leads to kinetic stabilization, and it is important to control the nuclearity of the cluster products. In addition, it is necessary to obtain  $[\text{Fe}_4\text{S}_4(\text{SR})_4]^{2-}$  and other degradation products to prevent the generation of ionic species from adding non-polar organics in the synthetic media. However, no  $[\text{Fe}_4\text{S}_4]^{4+}$  cluster carrying thiolates has been isolated from a one-electron-oxidized form of  $[\text{Fe}_4\text{S}_4(\text{SR})_4]^-$  with an  $[\text{Fe}_4\text{S}_4]^{3+}$  core [53]; that is to say, a reaction targeting  $[\text{Fe}_4\text{S}_4(\text{SR})_4]$  may likely be unstable. However, due to the short lifetimes of the reduced  $[\text{Fe}_4\text{S}_4(\text{SR})_4]^{4-}$  clusters, it is not clear whether the reactions are mediated by the all-ferrous cluster or by its decomposition products.

**Table 2.** Core oxidation state of  $[\text{Fe}_4\text{S}_4(\text{SR})_4]^{1-/2-/3-}$  analogues.

| Analogues                                   | R   | Year | Refs |
|---|---|------|------|
| $[\text{Fe}_4\text{S}_4(\text{SR})_4]^{1-}$ | Ph  | 1984 | [54] |
|   | $\text{CH}_2\text{Ph}$                                | 1994 | [55] |
|   | 2,4,6-triisopropylphenyl                              | 1985 | [56] |
|   | 2,6-di(mesityl)phenyl                                 | 1975 | [57] |
| $[\text{Fe}_4\text{S}_4(\text{SR})_4]^{2-}$ | H   | 1997 | [58] |
|   | Me  | 1974 | [59] |
|   | Bn  | 1972 | [41] |
|   | Ph  | 1974 | [60] |
|   | Et  | 2003 | [50] |
|   | $\text{CH}_3$   | 2014 | [61] |
|   | $\text{CH}_2\text{CH}_2\text{OH}$                     | 1999 | [62] |
|   | 2,3,4-pyridinemethane                                 | 2012 | [63] |
|   | 2,6-bis(acylamino)benzenethiolato                     | 1996 | [64] |
|   | $\text{CH}_2\text{CH}(\text{OH})\text{Me}$            | 2002 | [65] |
| $[\text{Fe}_4\text{S}_4(\text{SR})_4]^{3-}$ | $\text{CH}(\text{Me})\text{Ph}$                       | 2011 | [66] |
|   | $\text{CH}_2\text{CH}(\text{Me})\text{Et}$            |      |      |
|   | $\text{CH}_2\text{CH}(\text{OH})\text{CH}_2\text{OH}$ |      |      |
| $[\text{Fe}_4\text{S}_4(\text{SR})_4]^{3-}$ | H   | 1997 | [58] |
|   | Me  | 1988 | [67] |
|   | $\text{C}_6\text{H}_{11}$                             | 1986 | [68] |
|   | 4- $\text{BrC}_6\text{H}_4$                           | 1983 | [69] |
|   | $\text{CH}_2\text{Ph}$                                | 2015 | [70] |

The structural parameters for the synthetic analogues above of [4Fe4S] clusters are more precise than the protein-bound structure. A large amount of these synthetic cubane-type clusters will benefit researchers in understanding such synthetic clusters' two-electron transfer as proposed in nitrogenase.

## 4.2. Synthesizing Analogues of P-Clusters

### 4.2.1. Structure of P-Clusters

The P-cluster lies at the interface of  $\alpha$  and  $\beta$  subunits of the MoFe-protein and is held by three cysteine residues from each subunit. Two cysteine sulfur atoms bridge the two cubes; that is to say, the [8Fe7S] structure of P-cluster is constructed from two [4Fe4S] sub-clusters linked by a sulfide bonded to six ferritin atoms at one vertex [71]. This is likely assembled by the fusion of two [4Fe4S] sub-clusters [72] and has not been observed in any other biological system as an unusual  $\mu_6$ -S central atom. The reaction mechanism is well established in synthetic inorganic chemistry and was successfully realized by the synthesis of the P-cluster topology [50,73,74]. The paired [4Fe4S] clusters are likely the precursors to P-clusters which are obtained in the presence of reductant (i.e., dithionite) and ATP-dependent reductase (i.e., Fe-protein/MgATP) [75–77].

As a transfer station of electron sources in the enzymatic  $N_2$  fixation process, the P-cluster can transfer two electrons from the Fe-protein to the substrate reduction site of the FeMo-co, both of which are situated at an approximate distance of 15 Å to the Fe protein [78]. A two-electron transfer could explain the behavior of all nitrogenase substrates which reduce by an even number of electrons, as this is difficult to balance in a large amount of charge displacement. The protonation of substrates at the nitrogenase FeMo-co could be helpful in solving the above problem. One interesting possibility is that that Fe-protein binding is coupled to the coordination of S188 to the P-cluster lowering its potential and inducing electron transfer to FeMo-co and then “backfilling” by the Fe protein [79].

Being used in electron transfer, the reduced state of the P-cluster ( $P^N$ ) is thought to pass two electrons to the FeMo-co and change to an oxidized state ( $P^{OX}$ ) [78]. However, with accepting an electron from the Fe-protein, the P-cluster rapidly returns to the  $P^N$  state [79]. When the P-cluster oxidizes, significant conformational changes occur. The distance increases among the Fe atoms in the oxidation of the P-cluster [80]. For the spatial structure of the P-cluster, the average Fe–Fe bond distance increases from ~2.59 Å in the normal/reduced state to 2.88 Å in the oxidized state [15].

#### 4.2.2. Preparation of P-Clusters

The  $[Fe_8S_7]$  core of a P-cluster identified that the hexa-coordinate sulfur atom ( $\mu_6$ -S) is in the middle of its molecular space structure, and synthesizing Fe–S clusters with a  $\mu_6$ -sulfur atom became a hot research topic. The inorganic core of the P-cluster consists of two  $[Fe_4S_4]$  cubanes which are connected to each other through a disulfide bridge [81]. Respectively, the  $[Fe_4S_4]-(\mu-S)-[Fe_4S_4]$  cluster [82] and the edge-bridged  $[Fe_4S_4]-[Fe_4S_4]$  cluster [50] were early suggested as the bis- $[Fe_4S_4]$  core of the P-cluster (Figure 3). Actually, the P-cluster, located at the interface of the  $\alpha$  and  $\beta$  subunits of the MoFe-protein of nitrogenase, is a  $[Fe_8S_7]$  unit which is a bridge for the efficient transfer of electrons from the  $[4Fe4S]$  cluster of the Fe-protein to the FeMo-co of the MoFe-protein concomitant with MgATP hydrolysis [80].

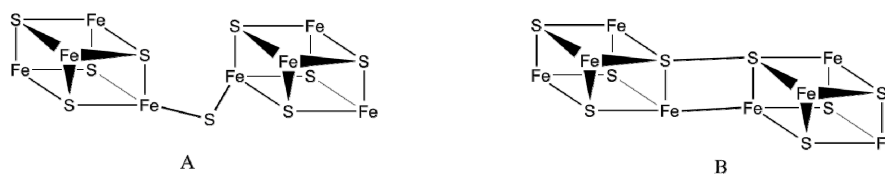


**Figure 3.** Cluster: (A)  $[Fe_4S_4]-(\mu-S)-[Fe_4S_4]$  and (B) edge-bridged  $[Fe_4S_4]-[Fe_4S_4]$ .

The P-cluster’s mediation of the reversible two-electron redox process has been demonstrated [83], exhibiting a one-electron reduction step for which the unique  $[Fe_4S_4]$  core of the P-cluster may be responsible. In addition, the  $[Fe_8S_7]$  core of the P-cluster could degrade into  $[Fe_4S_4]$  clusters in the presence of excess thiolate anions or thiols. This is consistent with the fact that 90–103% of non-cofactor ferritin content comes from the P-cluster [84], and the nitrogenase catalytic synthesizing  $NH_3$  process can be turned on/off via controlling the amount of reagents similar to thiols in the reaction solutions.

In a similar manner to the synthesis of the topological analogues to the P-cluster, Mo/Fe/S clusters with the P-cluster topology have been attained. The first Mo/Fe/S clusters  $[MoFe_3S_4]-[MoFe_3S_4]$  reacted with  $(Et_4N)(SH)$  to generate giant cluster  $[(Cl_4\text{-cat})_6Mo_6Fe_{20}S_{30}(Pet_3)_6]^{8-}$  ( $Cl_4\text{-cat}$ , a tetrachloro-catecholate ligand) crystals [85] which consist of  $Mo_2Fe_6S_9-Mo_2Fe_8S_{12}-Mo_2Fe_6S_9$  units. Here, the  $Mo_2Fe_6S_9$  unit is the  $[Fe_8S_7]$  cluster, a topological analogue to P-clusters. Another large cluster,  $[Mo_4Fe_{12}S_{18}]$ , was synthesized from a similar reaction of edge-bridged  $[MoFe_3S_4]-[MoFe_3S_4]$  cluster with  $(Et_4N)(SH)$  in the presence of reductant  $C_{14}H_{10}$  [86]. Although the two  $[Mo_2Fe_6S_9]$  clusters above differ from P-clusters in that they have molybdenum, their topology resembles the P-cluster core. The structure of  $[Mo_4Fe_{12}S_{18}]$  clusters with two  $Mo_2Fe_6S_9$  fragments linked by three potassium cations and two Fe- $(\mu-S)$ -Fe bridges is no more complicated than a  $[Mo_6Fe_{20}S_{30}]$  cluster with a  $[Mo_2Fe_6S_9]$  fragment that has an iso-structural relationship with the same unit in the  $[Mo_4Fe_{12}S_{18}]$  cluster [87].

### 4.3. Synthesizing Analogues of FeMo-co

#### 4.3.1. Structure of FeMo-co

The FeMo-co is the most complicated metallocluster known in nature [88]. With FeMo-co and its associated proteins being well-studied, one of the most intriguing things is its structural features [70]. The FeMo-co consists of a metallocluster with a molybdenum ion, seven Fe atoms, nine sulfur atoms, and one carbon atom as an interstitial ligand in the center termed "C" in Figure 1. The six Fe atoms form a trigonal prism around "C" with the sulfur surrounding the Fe atoms. However, the determination of the spatial structure of FeMo-co faces multiple barriers, as it does not expose all its exceptional catalytic properties for reducing  $N_2$  to  $NH_3$ .

Researchers have determined the structure of FeMo-co from nitrogenase many times over the decades. In 1992, Kim and Reed [89] presented the initial structure of FeMo-co consisting of  $[MoFe_3S_3]$  and  $[4Fe_4S]$  bridged by three sulfide ligands with a large, apparently empty, central cavity. However, the conclusion that carbon is the central atom was determined by multiple different studies using more detailed images from X-ray diffraction and more advanced ESEEM (electron spin-echo envelope modulation) [90]. The carbon in the active site may enable slight structural adaptations of the ferritin-core during turnover, and the binding of nitrogenase's natural substrate,  $N_2$ , to five-coordinate Fe complexes mimicking the FeMo-co's central carbon is also possible [91]. Therefore, Fe-carbon chemistry is important to  $N_2$  activation and reduction in general.

Until now, although FeMo-co has been thought of as the catalytic active site for reducing  $N_2$  to  $NH_3$ , the exact  $N_2$  reduction mechanism remains unknown. That is to say, the particular site at which the reduction of  $N_2$  on FeMo-co occurs is still incompletely confirmed. Perhaps the gap at element "C" (as shown in Figure 1) is the site of  $N_2$  reduction [15]; it is also possible that the  $N_2$  reduction takes place on the molybdenum [92] or ferritin ion [78].

Furthermore, keeping the stable spatial structure of FeMo-co analogues very similar to the biological FeMo-co, such as the assignment of the interstitial ligand, is significant to maintaining its catalytic activity for reducing  $N_2$  to  $NH_3$  under ambient conditions [11]. However, it is unnecessary for the major structural rearrangements during catalysis due to the interstitial ligands as carbon species. The interstitial carbon is a huge opportunity for the synthesis of FeMo-co analogues, because, in vitro, synthetic analogues of FeMo-co core metallocluster are difficult to achieve. Generally, nitrogenase's substrate  $N_2$  could possibly bind to five-coordinate Fe complexes mimicking the FeMo-co's central carbon [91], which requires the identification of the substrate binding site and the characterization of its various electronic states.

The FeMo-co is the most complex metallocluster known in nature. It is present at nitrogenase's active site and is recognized for its unique catalytic solution to reduce  $N_2$  to  $NH_3$ . However, FeMo-co extracted from nitrogenase into organic solvents cannot directly catalyze the reduction of  $N_2$  to  $NH_3$  due to the crucial influence of the protein matrix on its reactivity [93]. Therefore, the use of compounds such as Mo sources that act as ligands and redox reagents is significant for successfully synthesizing FeMo-co analogues whose stability and isolation are dependent on steric bulky groups of these donor ligands [52,94]. In recent years, much progress has been made in the synthesis of novel molybdenum- or ferritin-based analogues of FeMo-co reducing  $N_2$  to  $NH_3$ .

#### 4.3.2. Preparation of FeMo-co Analogues

One of the prerequisites for the preparation of FeMo-co analogues is to assemble eight Fe atoms with sulfur atoms like the P-cluster model, which is key to synthesizing large Fe-S clusters with more than four Fe atoms. Researchers tried to prompt a focus on reproducing this composition's stoichiometry of extracted FeMo-co, a synthetic complex [95]. So-called bis(thiolato)sulfide-bridged double cubanes  $[Mo_2Fe_6S_9(Se)_8]^{3-}$ , including two  $[MoFe_3S_4]$  units, were bridged via the Mo centers by inorganic sulfide and two thiolate ligands, to which  $[MoS_4]^{2-}$ ,  $FeCl_3$ , and  $NaSEt$  together contributed. The self-assembly reactions of  $[MoS_4]^{2-}/FeCl_3/NaSR$  resulted in forming double-cubane clusters,

[MoFe<sub>3</sub>S<sub>4</sub>]-[MoFe<sub>3</sub>S<sub>4</sub>], linked by ferritin–thiolate units [96]. The catalytic FeMo-co topology can be regarded as the fusion of Fe<sub>4</sub>S<sub>3</sub> and MoFe<sub>3</sub>S<sub>3</sub> units that are connected by three bridging μ<sub>2</sub>-S atoms and an interstitial μ<sub>6</sub>-C atom [97]. Functionally, a synthetic, trustworthy FeMo-co analogue must bind and reduce N<sub>2</sub> similarly to nitrogenase. Synthesis of FeMo-co analogues requires compounds reacting together as redox reagents and ligands which can play an important role in the stabilization and isolation of novel clusters due to the fact of their sterically bulky groups [95]. The substrate hydrogenation is not supported by the single-cubane models in the catalytic N<sub>2</sub> reduction process, thus the FeMo-co with double cubanes has efficient catalytic activity for reducing N<sub>2</sub> to NH<sub>3</sub> under ambient conditions [98]. Using [MoS<sub>4</sub>]<sup>2-</sup>, FeCl<sub>3</sub>, and NaSet as raw materials, a one-pot self-assembly reaction generated the [Mo<sub>2</sub>Fe<sub>6</sub>S<sub>9</sub>(Set)<sub>8</sub>]<sup>3-</sup> cluster containing two [MoFe<sub>3</sub>S<sub>4</sub>] units bridged via the Mo centers by inorganic sulfide and two thiolate ligands [99]. After identifying the unique dicubanoid structure of the FeMo-co, the synthesis of analogues shifted to modular approaches using the Mo cubane sources derived from [MoS<sub>4</sub>]<sup>2-</sup> as starting materials. The first edge-fused double cubane, [Mo<sub>2</sub>Fe<sub>6</sub>S<sub>8</sub>(Pet<sub>3</sub>)<sub>6</sub>(Cl<sub>4</sub>-cat)<sub>2</sub>], was attained via the reaction of [MoFe<sub>3</sub>S<sub>4</sub>Cl<sub>3</sub>(Cl<sub>4</sub>-cat)(NCMe)]<sup>2-</sup> with Pet<sub>3</sub> [100]. Then, a more discrete dicubane cluster, [Mo<sub>2</sub>Fe<sub>6</sub>S<sub>9</sub>(SH)<sub>2</sub>(Tp)<sub>2</sub>]<sup>3-</sup> (Tp = tris (pyrazoyl) borate), was generated from a related edge-bridged double cubane [101]. The [Fe<sub>8</sub>S<sub>6</sub>O(SDmp)<sub>4</sub>(OCPh<sub>3</sub>)] (SDmp = 2, 6-dimesitylphe-nylthiolate) cluster containing an interstitial u<sub>4</sub>-O<sup>2-</sup> atom has a more open double-cubanooid configuration than the others [99].

A large barrier is the presence of opposing peripheral Mo and Fe atoms in the FeMo-co analogue production process. The asymmetric core of the [Cp\*Mo<sup>IV</sup>Fe<sub>5</sub>S<sub>9</sub>(SH)]<sup>3-</sup> cluster was synthesized by the timely addition of [Cp\*MS<sub>3</sub>]<sup>-</sup> into a solution of hydrosulfide and FeCl<sub>2</sub> [51]. However, tiny alterations in the reaction conditions could influence the FeMo-co on the core configuration, such as obtaining the symmetric species [(Cp\*)<sub>2</sub>Mo<sub>2</sub>Fe<sub>4</sub>S<sub>9</sub>]<sup>2-</sup> by adding the reagents above in the reverse order. Correspondingly, DFT studies on Cp\*Fe(μ-Set)<sub>2</sub>FeCp\* suggest that the diferritin complex could catalyze the reduction of N<sub>2</sub> to NH<sub>3</sub> [102]. Here, the [Fe<sub>2</sub>S<sub>2</sub>] scaffold was effective in stabilizing nitrogenase donors [103]. Dance [104] mimicked the reduction of N<sub>2</sub> to NH<sub>3</sub> under mild conditions using three classes of known metal sulfide clusters that resemble the Nfe<sub>7</sub>MoS<sub>9</sub> core of FeMo-co. The three model systems possess an [Xfe<sub>4</sub>S<sub>4</sub>] face which is the key active site of FeMo-co (X is most probably N in FeMo-co and is S in the models).

Figure 4 shows that a molybdenum complex can convert N<sub>2</sub> to NH<sub>3</sub> only when the Mo oxidation states are more than III. Moreover, the ligand enclosing the molybdenum ion only permits small reactants such as nitrogen and protons to reach the active site. The system had cycled at least four times with an appropriate proton source and reductant [105]. Evidently, molybdenum can improve binding or protonation of the substrate by changing the electronic structure of FeMo-co.

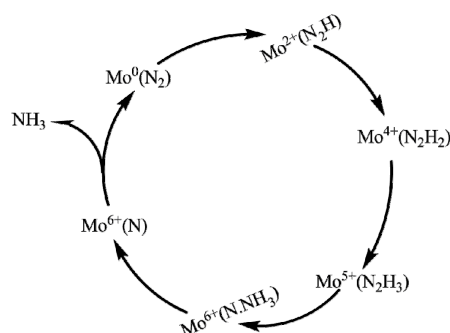


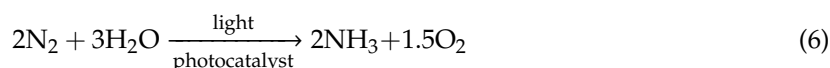
**Figure 4.** Different reduced nitrogen states with related molybdenum ions as catalytic active sites in the nitrogen reduction cycles.

Although molybdenum is usually regarded as a possible binding and cleavage site for N<sub>2</sub> reduction, it is difficult to judge whether the electronic structure of FeMo-co is relevant for the N<sub>2</sub> reduction taking place on this cofactor or not. Therefore, there is a hypothesis that the molybdenum

ion of FeMo-co would be the site for the last steps (E<sub>5</sub>–E<sub>8</sub>) of reducing N<sub>2</sub> to NH<sub>3</sub> in the cubane models as shown in Figure 2. With Co(Cp)<sub>2</sub> as electron donor and 2,6-lutidinium (Lu<sup>t</sup>-HCl) as a proton source, [MoFe<sub>3</sub>S<sub>4</sub>]<sup>3+</sup> cubanes catalyzed the 2e<sup>−</sup> reduction of hydrazine to NH<sub>3</sub> [106] as did the synthetic analogues with a [VFe<sub>3</sub>S<sub>4</sub>]<sup>2+</sup> core [107]. Theoretically, if ferritin is a possible substrate-binding site of MoFe-co, the first steps (E<sub>0</sub>–E<sub>4</sub>) (shown in Figure 2) toward reducing N<sub>2</sub> to NH<sub>3</sub> should occur on the Fe ion of FeMo-co, and the reaction intermediates would migrate from the Fe atom to the Mo atom.

#### 4.3.3. Synthesizing FeMo-co Analogues as Photo-Catalysts

Solar light as an energy source is a good choice for the photo-catalytic reduction of N<sub>2</sub> to NH<sub>3</sub> with water (H<sub>2</sub>O) as a reducing reagent under ambient conditions without fossil energy consumption and environmental pollution. Metal clusters embedded in the natural environment, such as the [Mn<sub>4</sub>O<sub>5</sub>Ca] cluster [108], can usually accomplish some complicated photo-catalytic redox reactions. This cluster changes the oxidation state, and controlling the redox potential is easy, as this type behaves similar to the Fe<sub>3</sub>/Al<sub>2</sub>O<sub>3</sub> cluster catalyst [109]. The photo-catalytic NH<sub>3</sub> production process mainly consists of the photo-catalytic oxidation of H<sub>2</sub>O to protons and the photo-catalytic reduction of N<sub>2</sub> to NH<sub>3</sub>. The mechanism steps are shown in Equations (4)–(6):



A photo-catalyst is dynamically converted between its oxidized and reduced states in the ammonia production process as shown in Figure 5. In this process, the amount of solar energy should be enough that it is absorbed and converted into the large free energy gain of N<sub>2</sub> to NH<sub>3</sub> ( $\Delta G^0 = 339 \text{ kJ mol}^{-1}$ ) [110]. That is to say, the photo-catalyst capable of oxidizing H<sub>2</sub>O (Equation (4)) can reduce N<sub>2</sub> by the photo-formed conduction band (CB) electrons (Equation (5)), producing NH<sub>3</sub> from N<sub>2</sub> and H<sub>2</sub>O (Equation (6)) under ambient conditions. Then, the CB position of the photo-catalysts should be more negative than the reduction potential of the N<sub>2</sub> hydrogenation; as well, the valance band (VB) should be more positive than the oxygen evolution potential, or the photo-generated holes must also be consumed to satisfy the charge neutrality (CB e<sup>−</sup> + VB h<sup>+</sup> = 0). Necessarily, a large thermodynamic driving force is required to overcome the N≡N band energy barrier for photo-catalytic synthesis of NH<sub>3</sub> from N<sub>2</sub> in solar light [111].

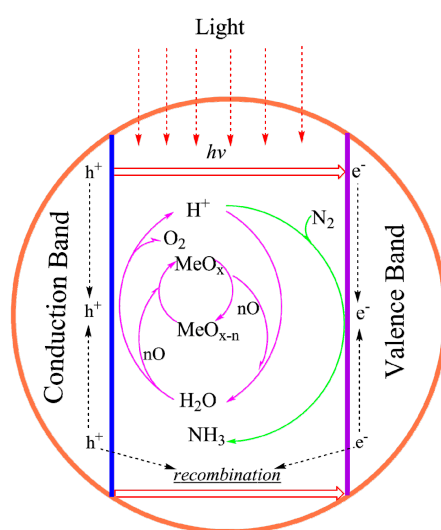


Figure 5. Schematic of metal cluster semiconductors as photocatalysts for reducing N<sub>2</sub> to NH<sub>3</sub> [112].

As the driving force, photons can actually promote the reduction of  $N_2$  to  $NH_3$  via multi-step injections of photo-generated electrons and  $H_2O$ -derived protons [113]. The first electron transfer ( $-4.16$  V versus NHE) and proton-coupled electron transfer ( $-3.2$  V versus NHE), shown in Table 3, must be overcome. Then, it is also necessary for the ideal photo-catalyst materials to have the characteristics of the charge carrier recombination and a small band gap in the visible light region.

**Table 3.** Redox potentials of reducing  $N_2$  to  $NH_3$  [112].

| No. | Reaction                                | $E^0$ (V)            |
|-----|---|----------------------|
| 1   | $H_2O + 2h^+ \rightarrow 0.5O_2 + 2H^+$ | 1.33 <sup>b</sup>    |
| 2   | $H^+ + e^- \rightarrow 0.5H_2$          | $-0.42$ <sup>a</sup> |
| 3   | $N_2 + e^- \rightarrow N_2^-$           | $-4.16$ <sup>b</sup> |
| 4   | $N_2 + H^+ + e^- \rightarrow N_2H$      | $-3.2$ <sup>b</sup>  |
| 5   | $N_2 + 6H^+ + 6e^- \rightarrow 2NH_3$   | 0.55 <sup>b</sup>    |

<sup>a</sup> $E^0$  versus NHE at pH 7; <sup>b</sup> $E^0$  versus NHE at pH 0. (NHE, Normal Hydrogen Electrode).

The biohybrids of CdS and the polyatomic metal cluster of the MoFe-protein provide a photo-chemical model for achieving light-driven catalyzation of the reaction process. Katherine et al. [114] reported that cadmium sulfide (CdS) nanocrystals can be used to drive the enzymatic reduction of  $N_2$  to  $NH_3$  by photosensitizing the MoFe-protein of nitrogenase, not ATP hydrolysis. Under optimal conditions, the turnover rate was 75 per minute, 63% of the ATP-coupled reaction rate for the nitrogenase complex. In addition, the biohybrids of the CdS and MoFe-protein provide a photochemical model for achieving light-driven catalyzation of the reaction process. In this process, Fe is necessary, but Mo is not; however, this does not mean Mo does not play a role in  $N_2$  binding.

A redox-flexible metal center can adjust the oxidation state of the active center metal and the redox potentials in different steps of the LT model such as Mn, Fe, Co, Ni, and Mo. Results [115] suggest that nitrogenase could keep its photo-catalytic activity when the [4Fe4S] clusters are replaced with other inert ions such as  $Sb^{3+}$ ,  $Sn^{4+}$ , and  $Zn^{2+}$ . For example, both  $[Mo_2Fe_6S_8(SPh)_3]$  and [4Fe4S] clusters [112,116] in nitrogenase could do so at ambient temperature and pressure. Therefore, redox-active iron-sulfide-containing clusters with high-energy photo-excited states could photo-catalyze the reduction of  $N_2$  to  $NH_3$ . Both the reduction potential of the adsorbate and the position of the energy band are important for making a decision on the photo-catalyst materials used for reducing  $N_2$  to  $NH_3$  under ambient conditions.

#### 4.3.4. Incorporating Carbon Atoms into FeMo-co Analogues

As shown in Figure 1, the FeMo-co consists of a molybdenum ion, seven Fe atoms, nine sulfur atoms, and one carbon atom as an interstitial ligand in the center termed "C". Embedding a carbon donor into analogues of the FeMo-co as an interstitial carbon for mimicking the biological nitrogenase is especially challenging. Xu et al. [117] reported that a core halide ligand ( $Cl^-$  or  $Br^-$ ) replacing thiolate was incorporated into a binding site of the heterometallic clusters using one-electron reductant sodium benzophenone ketyl. The new approach provided opportunities to synthesize the analogues more similar to FeMo-co, because core halides are easily replaced with carbon ligands through metathesis reactions.

The carbide ligand in the FeMo-co is obtained by a methyl group transferring from S-adenosyl methionine [21]. Therefore, methyl anion incorporated into an incomplete cubane might bridge the methyl ligand through salt metathesis or oxidative metathesis. As mentioned above, with all-sulfide clusters dimerizing in the presence of a reductant, the formation of the edge-bridged (bis) cubanes is available, then addition of thiolate sources could cause rearrangement to form corner-sharing (bis) cubanes with the topology of the FeMo-co [118]. The ability to introduce carbon into synthetic Fe-S clusters with the topology of the FeMo-co may provide insight into the influence of the carbide in  $N_2$  reduction [119].

## 5. Summary and Outlook

Nitrogenase metalloclusters, namely, the [4Fe4S] cluster, P-cluster, and FeMo-co, are indispensable for biological reduction of N<sub>2</sub> to NH<sub>3</sub> at room temperature and atmospheric pressure. Although synthetic analogues of nitrogenase metalloclusters are promising artificial catalytic clusters due to the fact of their intriguing features, no synthesized clusters have yet been entirely similar to the biogenic clusters. Accurate synthesis of nitrogenase metallocluster analogues that can activate the strong bond of N<sub>2</sub> at ambient conditions is an important step to accomplish this kind of catalyst design. Synthetic methods involve ferritin halides (FeCl<sub>2</sub> or FeCl<sub>3</sub>) with thiolates and sulfide sources (e.g., HS<sup>-</sup>, S<sup>2-</sup>) in polar organic solvents such as methanol and DMF. The spontaneous assembly of ferritin atoms in the presence of sulfur reagents is an efficient and common method for synthesizing [4Fe4S] clusters. The spontaneous assembly reactions would be terminal when the Fe–S cluster products become stable. The inorganic [Fe<sub>8</sub>S<sub>7</sub>] core of P-clusters consists of two [4Fe4S] cubanes which are connected to each other through a disulfide bridge. Different approaches to synthesizing analogues of the P-cluster have been carried out and much progress has been made. In a non-polar organic solvent, the [8Fe7S] cluster can be produced from the self-assembly reaction. Topological analogues of the P-cluster can be obtained from the core rearrangement reactions of [MoFe<sub>3</sub>S<sub>4</sub>]-[MoFe<sub>3</sub>S<sub>4</sub>] clusters. In addition, the [8Fe7S] core of the P-cluster could degrade into [4Fe4S] clusters in the presence of excess thiolate anions or thiols. There is no doubt that the synthetic analogues of the P-cluster can be compared to the structures and properties of the native clusters. Although much progress on synthesizing FeMo-co analogues have been reported in the past decades, no synthesized analogues of FeMo-co clusters have been completely similar to the biogenic clusters, especially concerning their catalysis, functionality, and capacity aspects. The synthesis of FeMo-co analogues remains a large challenge. The successful synthesis of FeMo-co analogues depends on redox reagents and ligands whose steric bulky groups are good for the stability and isolation of synthetic analogues. Besides these redox reagents and ligands, the appropriate arrangement of a variety of elements, such as molybdenum, ferritin, and sulfur in the cores of FeMo-co analogue clusters, is still a challenging problem which has to be solved. Based on this, the construction of other transition metal–sulfur clusters for generating complicated cluster structures in non-polar solvents may be a good choice for an NH<sub>3</sub> production process under ambient conditions. As more insights into the structures and function of FeMo-co become available, more reliable synthetic models will emerge to gain synthetic analogues with efficient catalytic activity in NH<sub>3</sub> synthesis. No viable and efficient catalysts for sustainable NH<sub>3</sub> synthesis could meet all the requirements of an active, selective, scalable, long-lived catalyst, and discovering novel catalysts which need new design approaches is a major challenge. For example, insight from heterogeneous, homogeneous, enzyme catalysis, and computational methods of atomic-scale controlled synthesis, if combined, could strengthen the possibilities for a break-through in NH<sub>3</sub>-synthetic catalyst design. Basically, novel catalyst design approaches should be based on the characterization of the active catalyst, reaction intermediates, and the relevant bond energies as well as the effects of the reaction media. Synthetic analogues of [4Fe4S], the P-cluster, and the FeMo-cofactor that can reduce known nitrogenase substrates would be valuable in better understanding the reactivity of N<sub>2</sub> reduction under ambient conditions.

**Funding:** This work was supported by the China Scholarship Council (No. 201706565033).

**Conflicts of Interest:** The author declares no conflict of interest.

## References

1. Kandemir, T.; Schuster, M.E.; Senyshyn, A.; Behrens, M.; Schlögl, R. The Haber-Bosch Process Revisited: On the Real Structure and Stability of “Ammonia Ferritin” under Working Conditions. *Angew. Chem. Int. Ed.* **2013**, *52*, 12723. [[CrossRef](#)] [[PubMed](#)]
2. Shipman, M.A.; Symes, M.D. Recent progress towards the electro-synthesis of ammonia from sustainable resources. *Cata. Today* **2017**, *286*, 57–68. [[CrossRef](#)]

3. Haber, F.; Leiser, R. Method and Apparatus for Testing Gases. Patent US1269599A, 18 June 1918.
4. Bosch, C. The development of the chemical high pressure method during the establishment of the new ammonia industry. *Nobel Lect.* **1932**, *1941*, 197–235.
5. Tamaru, K. *Catalytic Ammonia Synthesis: Fundamentals and Practice*; Plenum Press: New York, NY, USA, 1991.
6. Galloway, J.N.; Cowling, E.B. Reactive N<sub>2</sub> and The World: 200 Years of Change, *AMBIO. J. Hum. Environ.* **2002**, *31*, 64–71. [[CrossRef](#)] [[PubMed](#)]
7. Galloway, J.N. N<sub>2</sub> Cycles: Past, Present and Future. *Biogeochemistry* **2004**, *70*, 153–226. [[CrossRef](#)]
8. Erisman, J.W.; Bleeker, A.; Galloway, J.; Sutton, M.S. Reduced N<sub>2</sub> in ecology and the environment. *Environ. Pollut.* **2007**, *150*, 140–149. [[CrossRef](#)]
9. Giddey, S.; Badwal, P.S.; Kulkarni, A. Review of electrochemical ammonia production technologies and materials. *Inter. J. Hydro. Energy* **2013**, *38*, 14576–14594. [[CrossRef](#)]
10. Schlögl, R. Catalytic Synthesis of Ammonia-A “Never-Ending Story”? *Angew. Chem. Int. Ed.* **2003**, *42*, 2004–2008. [[CrossRef](#)]
11. Spatzal, T. Reactive Nitrogen-Containing Species: Generation, Characterization and Functionalization. *J. Inorg. Gen. Chem.* **2015**, *641*, 1–135.
12. Garagounis, I.; Kyriakou, V.; Skodra, A.; Vasileiou, E.; Stoukides, M. Electrochemical synthesis of ammonia in solid electrolyte cells. *Front. Energy Res.* **2014**, *2*, 1–10. [[CrossRef](#)]
13. Amar, I.A.; Lan, R.; Petit, C.T.G.; Tao, S.W. Solid-state electrochemical synthesis of ammonia: A review. *J. Solid State Electrochem.* **2011**, *15*, 1845–1860. [[CrossRef](#)]
14. Erisman, J.W.; Sutton, M.A.; Galloway, J.; Klimont, Z.; Winiwarter, W. How a century of ammonia synthesis changed the world. *Nat. Geosci.* **2008**, *1*, 636–639. [[CrossRef](#)]
15. Hoffman, B.M.; Lukoyanov, D.; Yang, Z.Y.; Dean, D.R.; Seefeldt, L.C. Mechanism of N<sub>2</sub> fixation by Nitrogenase: The next stage. *Chem. Rev.* **2014**, *114*, 4041–4062. [[CrossRef](#)] [[PubMed](#)]
16. Burgess, B.K.; Lowe, D.J. Mechanism of Molybdenum Nitrogenase. *Chem. Rev.* **1996**, *96*, 2983–3011. [[CrossRef](#)] [[PubMed](#)]
17. Modak, J.M. Haber process for ammonia synthesis. *Resonance* **2002**, *7*, 69–77. [[CrossRef](#)]
18. Khoenkhoen, N.; de Bruin, B.; Reek, J.N.; Dzik, W.I. Reactivity of DiN<sub>2</sub> Bound to Mid—and Late-Transition-Metal Centres. *Eur. J. Inorg. Chem.* **2015**, *4*, 567–598. [[CrossRef](#)]
19. Georgiadis, M.M.; Komiya, H.; Chakrabarti, P.; Woo, D.; Kornuc, J.J.; Rees, D.C. Crystallographic structure of the nitrogenase ferritin protein from *Azotobacter vinelandii*. *Science* **1992**, *257*, 1653–1659. [[CrossRef](#)]
20. Wiig, J.A.; Hu, Y.; Lee, C.C.; Ribbe, M.W. Radical SAM-Dependent Carbon Insertion into the Nitrogenase FeMo-co. *Science* **2012**, *337*, 1672–1675. [[CrossRef](#)]
21. Seefeldt, L.C.; Dean, D.R.; Hoffman, B.M. Nitrogenase Mechanism: Electron and Proton Accumulation and N<sub>2</sub> Reduction. In *Molybdenum and Tungsten Enzymes: Biochemistry*; Royal Society of Chemistry: London, UK, 2017.
22. Simpson, F.B.; Burris, R.H. A nitrogen pressure of 50 atmospheres does not prevent evolution of hydrogen by nitrogenase. *Science* **1984**, *224*, 1095–1097. [[CrossRef](#)]
23. Bjornsson, R.; Delgado-Jaime, M.U.; Lima, F.A.; Sippel, D.; Schlesier, J.; Weyhermüller, T.; Einsle, O.; Neese, F.; DeBeer, S. Molybdenum L-Edge XAS Spectra of MoFe Nitrogenase. *Z. Anorg. Allg. Chem.* **2015**, *641*, 65–71. [[CrossRef](#)]
24. Grossman, J.G.; Hasnain, S.S.; Yousafzai, F.K.; Smith, B.E.; Eady, R.R. Comparing crystallographic and solution structures of nitrogenase complexes. *Acta. Crystallogr.* **1999**, *55*, 727–728. [[CrossRef](#)] [[PubMed](#)]
25. Chiu, H.J.; Peters, J.W.; Lanzilotta, W.N.; Ryle, M.J.; Seefeldt, L.C. MgATP-bound and nucleotide-free structures of a nitrogenase protein complex between the Leu127-Fe-protein and the MoFe-protein. *Biogeochemistry* **2001**, *40*, 641–650. [[CrossRef](#)] [[PubMed](#)]
26. Yang, Z.Y.; Danyal, K.; Seefeldt, L.C. *Nitrogen Fixation: Mechanism of Mo-Dependent Nitrogenase*; Springer: Berlin, Germany, 2011.
27. Tezcan, F.A.; Kaiser, J.T.; Mustafi, D.; Walton, M.Y.; Howard, J.B.; Rees, D.C. Nitrogenase Complexes: Multiple Docking Sites for a Nucleotide Switch Protein. *Science* **2005**, *309*, 1377–1380. [[CrossRef](#)] [[PubMed](#)]
28. Tezcan, F.A.; Kaiser, J.T.; Howard, J.B.; Rees, D.C. Structural Evidence for Asymmetrical Nucleotide Interactions in Nitrogenase. *J. Am. Chem. Soc.* **2015**, *137*, 146–149. [[CrossRef](#)]

29. Lukoyanov, D.; Khadka, N.; Dean, D.R.; Raugei, S.; Seefeldt, L.C.; Hoffman, B.M. Photoinduced Reductive Elimination of H<sub>2</sub> from the Nitrogenase Dihydride (Janus) State Involves a FeMo-cofactor-H<sub>2</sub> Intermediate. *Inorg. Chem.* **2017**, *56*, 2233–2240. [[CrossRef](#)]
30. Thorneley, R.N.; Lowe, D.J. The mechanism of *Klebsiella pneumoniae* nitrogenase action. *J. Biochem.* **1984**, *224*, 887–894. [[CrossRef](#)]
31. Watt, G.D.; Reddy, K.R.N. Formation of an all ferrous Fe<sub>4</sub>S<sub>4</sub> cluster in the ferritin protein component of *Azotobacter vinelandii* Nitrogenase. *J. Inorg. Biochem.* **1994**, *53*, 281–294. [[CrossRef](#)]
32. Siegbahn, P. The mechanism for nitrogenase including all steps. *Phys. Chem. Chem. Phys.* **2019**, *21*, 15747–15759. [[CrossRef](#)]
33. Kaczmarek, M.A.; Malhotra, A.; Balan, G.A.; Timmins, A.; de Visser, S.P. Nitrogen Reduction to Ammonia on a Biomimetic Mononuclear Iron Centre: Insights into the Nitrogenase Enzyme. *Chem. Eur. J.* **2018**, *24*, 5293–5302. [[CrossRef](#)]
34. Benedek, Z.; Papp, M.; Oláh, J.; Szilvási, T. Identifying the Rate-Limiting Elementary Steps of Nitrogen Fixation with Single-Site Fe Model Complexes. *Inorg. Chem.* **2018**, *57*, 8499–8508. [[CrossRef](#)]
35. Sickerman, N.S.; Tanifuji, K.; Hu, Y.L.; Ribbe, M.W. Synthetic Analogues of Nitrogenase Metallocofactors: Challenges and Developments. *Eur. J. Chem.* **2017**, *23*, 12425–12432. [[CrossRef](#)] [[PubMed](#)]
36. Ribbe, M.W.; Hu, Y.; Hodgson, K.O.; Hedman, C. *Chem. Rev.* **2014**, *114*, 4063–4080. [[CrossRef](#)] [[PubMed](#)]
37. Bazhenova, T.; Shilov, A. Nitrogen fixation in solution coordination. *Chem. Rev.* **1995**, *144*, 69–145.
38. Lanzilotta, W. Nucleotide hydrolysis and protein conformational changes in *azotobacter*. *Biochemistry* **1995**, *34*, 10713–10723. [[CrossRef](#)] [[PubMed](#)]
39. Nyborg, A.; Johnson, J.; Gunn, A.; Watt, G. Evidence for a two-electron transfer using the all-ferrous Fe-protein during nitrogenase catalysis. *J. Biol. Chem.* **2000**, *275*, 39307–39312. [[CrossRef](#)]
40. Schindelin, H.; Kisker, C.; Schlessman, J.L.; Howard, J.B.; Rees, D.C. Structure of ADP·AlF<sub>4</sub><sup>−</sup>-stabilized nitrogenase complex and its implications for signal transduction. *Nature* **1997**, *387*, 370–376. [[CrossRef](#)]
41. Herskovitz, T.; Averill, B.A.; Holm, R.H.; Ibers, J.A.; Phillips, W.D.; Weiher, J.F. Structure and Properties of a Synthetic Analogue of Bacterial Ferritin-Sulfur Proteins. *Proc. Natl. Acad. Sci. USA* **1972**, *69*, 2437–2441. [[CrossRef](#)]
42. Rao, P.V.; Holm, R.H. Synthetic Analogues of the Active Sites of Ferritin-Sulfur Proteins. *Chem. Rev.* **2004**, *104*, 527–559.
43. Hagen, K.S.; Watson, A.D.; Holm, R.H. Synthetic Routes to Fe<sub>2</sub>S<sub>2</sub>, Fe<sub>3</sub>S<sub>4</sub>, Fe<sub>4</sub>S<sub>4</sub>, and Fe<sub>6</sub>S<sub>6</sub> Clusters from the Common Precursor [Fe(SC<sub>2</sub>H<sub>5</sub>)<sub>4</sub>]<sup>2−</sup>: Structures and Properties of [Fe<sub>3</sub>S<sub>4</sub>(SR)]<sup>3−</sup> and [Fe<sub>6</sub>(SC<sub>2</sub>H<sub>5</sub>)<sub>2</sub>]<sup>4−</sup>, Examples of the Newest Types of Fe-S-SR Clusters. *J. Am. Chem. Soc.* **1983**, *105*, 3905–3913.
44. Cambray, J.; Lane, R.W.; Wedd, A.G.; Johnson, R.W.; Holm, R.H. Chemical and Electrochemical Interrelationships of the 1-Fe, 2-Fe, and 4-Fe Analogues of the Active Sites of Ferritin-Sulfur Proteins. *Inorg. Chem.* **1977**, *16*, 2565–2571. [[CrossRef](#)]
45. McSkimming, A.; Daniel, L.M. Selective Synthesis of Site-Differentiated Fe<sub>4</sub>S<sub>4</sub> and Fe<sub>6</sub>S<sub>6</sub> Clusters. *Inorg. Chem.* **2018**, *57*, 14904–14912. [[CrossRef](#)] [[PubMed](#)]
46. Ohki, Y.; Tanifuji, K.; Yamada, N.; Imada, M.; Tajima, T.; Tatsumi, K. Synthetic analogues of [Fe<sub>4</sub>S<sub>4</sub>(Cys)<sub>3</sub>(His)] in hydrogenases and [Fe<sub>4</sub>S<sub>4</sub>(Cys)<sub>4</sub>] in HiPIP derived from all-ferric [Fe<sub>4</sub>S<sub>4</sub>{N(SiMe<sub>3</sub>)<sub>2</sub>]<sub>4</sub>]. *Proc. Natl. Acad. Sci. USA* **2011**, *108*, 12635–12640. [[CrossRef](#)] [[PubMed](#)]
47. Wong, G.B.; Bobrik, M.A.; Holm, R.H. Inorganic Derivatives of Ferritin Sulfide Thiolate Dimers and Tetramers: Synthesis and Properties of the Halide Series [Fe<sub>2</sub>S<sub>2</sub>X<sub>4</sub>]<sup>2−</sup> and [Fe<sub>4</sub>S<sub>4</sub>X<sub>4</sub>]<sup>2−</sup> (X = Cl, Br, I). *Inorg. Chem.* **1978**, *17*, 578. [[CrossRef](#)]
48. Tyson, M.A.; Demadis, K.D.; Coucouvanis, D. Uncharged Mixed-Ligand Clusters with the [Fe<sub>4</sub>S<sub>4</sub>]<sup>+</sup> and [Fe<sub>4</sub>S<sub>4</sub>]<sup>2+</sup> Cores. Synthesis, Structural Characterization, and Properties of the Fe<sub>4</sub>S<sub>4</sub>X(†Bu<sub>3</sub>P)<sub>3</sub> (X = Cl, Br, I) and Fe<sub>4</sub>S<sub>4</sub>(SPh)<sub>2</sub>(†Bu<sub>3</sub>P)<sub>2</sub> Cubanes. *Inorg. Chem.* **1995**, *34*, 4519. [[CrossRef](#)]
49. Zhou, H.C.; Holm, R.H. Synthesis and reactions of cubane-type ferritin-sulfurphosphine clusters, including soluble clusters of nuclearities 8 and 16. *Inorg. Chem.* **2003**, *42*, 11–21. [[CrossRef](#)] [[PubMed](#)]
50. Goh, C.; Segal, B.M.; Huang, J.S.; Long, J.R.; Holm, R.H. Polycubane Clusters: Synthesis of [Fe<sub>4</sub>S<sub>4</sub>(PR<sub>3</sub>)<sub>4</sub>]<sup>1+,0</sup> (R = But, Cy, Pri) and [Fe<sub>4</sub>S<sub>4</sub>]<sup>0</sup> Core Aggregation upon Loss of Phosphine. *J. Am. Chem. Soc.* **1996**, *118*, 11844. [[CrossRef](#)]

51. Tanifuji, K.; Yamada, N.; Tajima, T.; Sasamori, T.; Tokitoh, N.; Matsuo, T.; Tamao, K.; Ohki, Y.; Tatsumi, K. A convenient route to synthetic analogues of the oxidized form of high-potential iron–sulfur proteins. *Inorg. Chem.* **2014**, *53*, 4000–4009. [[CrossRef](#)]
52. Ohta, S.; Ohki, Y. Impact of ligands and media on the structure and properties of biological and biomimetic iron-sulfur clusters. *Coord. Chem. Rev.* **2017**, *338*, 207–225. [[CrossRef](#)]
53. Cleland, W.E.; Holtman, D.A.; Sabat, M.; Ibers, J.A.; DeFotis, G.C.; Averill, B.A. Effects of Phenoxide Ligation on Iron-Sulfur Clusters: Preparation and Properties of  $[\text{Fe}_4\text{S}_4(\text{OAr})_4]^{2-}$  Ions and the Structure of  $[(\text{C}_2\text{H}_5)_4\text{N}]_2[\text{Fe}_4\text{S}_4(\text{OC}_6\text{H}_5)_4]$ . *J. Am. Chem. Soc.* **1983**, *105*, 6021. [[CrossRef](#)]
54. Gaillard, J.; Gloux, J.; Gloux, P.; Lamotte, B.; Rius, G. Elucidation of the microscopic mechanism of ferroelectricity and of the associated phase transition from high resolution nmr of  $^{31}\text{p}$  in a new hydrogen-bonded ferroelectric: Ammonium phosphotellurate. *Ferroelectrics* **1984**, *54*, 6. [[CrossRef](#)]
55. Gloux, J.; Gloux, P.; Lamotte, B.; Mouesca, J.M.; Rius, G. The Different  $[\text{Fe}_4\text{S}_4]^{3+}$  and  $[\text{Fe}_4\text{S}_4]^+$  Species Created by Gamma. Irradiation in Single Crystals of the  $(\text{Et}_4\text{N})_2[\text{Fe}_4\text{S}_4(\text{SBenz})_4]$  Model Compound: Their EPR Description and Their Biological Significance. *J. Am. Chem. Soc.* **1994**, *116*, 1953–1961. [[CrossRef](#)]
56. O’Sullivan, T.; Millar, M.M. Synthesis and study of an analog for the  $[\text{Fe}_4\text{S}_4]^{3+}$  center of oxidized high potential iron-sulfur proteins. *J. Am. Chem. Soc.* **1985**, *107*, 4096–4097. [[CrossRef](#)]
57. Adman, E.; Watenpaugh, K.D.; Jensen, L.H. NH—S hydrogen bonds in Peptococcus aerogenes ferredoxin, Clostridium pasteurianum rubredoxin and Chromatium high potential iron protein. *Proc. Natl. Acad. Sci. USA* **1975**, *72*, 4854–4858. [[CrossRef](#)] [[PubMed](#)]
58. Hoveyda, H.R.; Holm, R.H. Characterization of the Self-Condensation Equilibrium of  $[\text{Fe}_4\text{S}_4(\text{SH})_4]^{2-}$ : Spectroscopic Identification of a Unique Sulfido-Bridged Acyclic Tricubane Cluster. *Inorg. Chem.* **1997**, *36*, 4571. [[CrossRef](#)] [[PubMed](#)]
59. Holm, R.H.; Phillips, W.D.; Averill, B.A.; Mayerle, J.J.; Herskovitz, T. Synthetic analogs of the active sites of iron-sulfur proteins. V. Proton resonance properties of the tetranuclear clusters  $[\text{tetra-}\mu\text{-sulfido-tetrakis(alkyl or aryl thiolato)tetraferate}]^{2-}$ . *J. Am. Chem. Soc.* **1974**, *96*, 2109–2117. [[CrossRef](#)] [[PubMed](#)]
60. Que, L.J.; Bobrik, M.A.; Ibers, J.A.; Holm, R.H. Synthetic analogs of the active sites of iron-sulfur proteins. VII. Ligand substitution reactions of the tetranuclear clusters  $(\text{Fe}_4\text{S}_4(\text{SR})_4)^{2-}$  and the structure of  $((\text{CH}_3)_4\text{N})_2(\text{Fe}_4\text{S}_4(\text{SC}_6\text{H}_5)_4)$ . *J. Am. Chem. Soc.* **1974**, *96*, 4168–4178. [[CrossRef](#)]
61. Sharma, S.; Sivalingam, K.; Garnet, F.N.; Chan, K.L. Low-energy spectrum of iron-sulfur clusters directly from many-particle quantum mechanics. *Nat. Chem.* **2014**, *6*, 927–933. [[CrossRef](#)]
62. Barclay, J.E.; Davies, S.C.; Evans, D.J.; Hughes, D.L.; Longhurst, S. Lattice effects in the Mössbauer spectra of salts of  $[\text{Fe}_4\text{S}_4\{\text{S}(\text{CH}_2)_n\text{OH}_4\}]^{2-}$ . Crystal structures of  $[\text{PPh}_4]_2[\text{Fe}_4\text{S}_4\{\text{S}(\text{CH}_2)_n\text{OH}_4\}]$  ( $n = 2, 3$  and  $4$ ). *Inorg. Chim. Acta.* **1999**, *291*, 101. [[CrossRef](#)]
63. Kim, Y.; Han, J. Synthesis, Structure, and Reactivity of the  $[\text{Fe}_4\text{S}_4(\text{SR})_4]^{2-}$  ( $R = 2\text{-}, 3\text{-}, 4\text{-Pyridinemethane}$ ) Clusters. *Bul. Korean Chem. Soc.* **2012**, *33*, 48–54. [[CrossRef](#)]
64. Ueyama, N.; Yamada, Y.; Okamura, T.; Kimura, S.; Nakamura, A. Structure and Properties of  $[\text{Fe}_4\text{S}_4\{2,6\text{-bis(acetylamino)benzenethiolato-S}_4\}]^{2-}$  and  $[\text{Fe}_2\text{S}_2\{2,6\text{-bis(acetylamino)benzenethiolato-S}_4\}]^{2-}$ : Protection of the Fe-S Bond by Double NH-S Hydrogen Bonds. *Inorg. Chem.* **1996**, *35*, 6473–6484. [[CrossRef](#)]
65. Davies, S.C.; Evans, D.J.; Henderson, R.A.; Hughes, D.L.; Longhurst, S. Mononuclear, binuclear, trinuclear and tetranuclear iron complexes of the  $\text{N}(\text{CH}_2\text{CH}_2\text{S})_3^{3-}$  ( $\text{NS}_3$ ) ligand with nitrosyl co-ligands. *J. Chem. Soc. Dalton Trans.* **2002**, *43*, 2473–2482. [[CrossRef](#)]
66. Lo, W.; Huang, S.; Zheng, S.L.; Holm, R.H. Cubane-type  $\text{Fe}_4\text{S}_4$  Clusters with Chiral Thiolate Ligation: Formation by Ligand Substitution, Detection of Intermediates by  $^1\text{H}$  NMR, and Solid State Structures Including Spontaneous Resolution Upon Crystallization. *Inorg. Chem.* **2011**, *50*, 11082–11090. [[CrossRef](#)] [[PubMed](#)]
67. Carney, M.J.; Papaefthymiou, G.C.; Spartalian, K.; Frankel, R.B.; Holm, R.H. Ground spin state variability in  $[\text{Fe}_4\text{S}_4(\text{SR})_4]^{3-}$  synthetic analogs of the reduced clusters in ferredoxins and other iron-sulfur proteins: Cases of extreme sensitivity of electronic state and structure to extrinsic factors. *J. Am. Chem. Soc.* **1988**, *110*, 6084–6095. [[CrossRef](#)] [[PubMed](#)]
68. Münck, E.; Kent, T.A. Structure and magnetism of iron-sulfur clusters in proteins. *Hyperfine Interact.* **1986**, *27*, 161–172. [[CrossRef](#)]

69. Stephan, D.W.; Papaefthymiou, G.C.; Frankel, R.B.; Holm, R.H. Analogues of the  $(4\text{Fe-4S})^+$  sites of reduced ferredoxins: Structural and spectroscopic properties of  $((\text{C}_2\text{H}_5)_4\text{N})_3(\text{Fe}_4\text{S}_4(\text{S-P-C}_6\text{H}_4\text{Br})_4)$  in crystalline and solution phases. *Inorg. Chem.* **1983**, *22*, 1550. [[CrossRef](#)]
70. Lee, C.C.; Fay, A.W.; Weng, T.-C.; Krest, C.M.; Hedman, B.; Hodgson, K.O.; Hu, Y.; Ribbe, M.W. Uncoupling binding of substrate CO from turnover by vanadium nitrogenase. *Proc. Natl. Acad. Sci. USA* **2015**, *112*, 13845–13849. [[CrossRef](#)]
71. Henderson, R.A. *N<sub>2</sub> Fixation at the Millenium: Advances Towards the Mechanism of Nitrogenases*; Elsevier: Amsterdam, The Netherlands, 2002; pp. 223–261.
72. Hu, Y.; Fay, A.W.; Lee, C.C.; Yoshizawa, J.; Ribbe, M.W. Assembly of Nitrogenase MoFe-protein. *Biogeochemistry* **2008**, *47*, 3973–3981. [[CrossRef](#)]
73. Zhang, Y.; Holm, R.H. Structural conversions of molybdenum-ferritin-sulfur edge-bridged double cubanes and  $\text{P}^{\text{N}}$ -type clusters topologically related to the nitrogenase P-cluster. *Inorg. Chem.* **2004**, *43*, 674–682. [[CrossRef](#)]
74. Hlavinka, M.L.; Miyaji, T.; Staples, R.J.; Holm, R.H. Hydroxide-promoted core conversions of molybdenum-ferritin-sulfur edge-bridged double cubanes: Oxygen-ligated topological  $\text{P}^{\text{N}}$  clusters. *Inorg. Chem.* **2007**, *46*, 9192–9200. [[CrossRef](#)]
75. Corbett, M.C. Comparison of ferritin-molybdenum cofactor-deficient nitrogenase MoFe-proteins by X-ray absorption spectroscopy: Implications for P-cluster biosynthesis. *J. Biol. Chem.* **2004**, *279*, 28276–28282. [[CrossRef](#)]
76. Broach, R.B. Variable-temperature, variable-field magnetic circular dichroism spectroscopic study of the metal clusters in the nifB and nifH MoFe-proteins of nitrogenase from *Azotobacter vinelandii*. *Biogeochemistry* **2006**, *45*, 15039–15048. [[CrossRef](#)] [[PubMed](#)]
77. Hu, Y. Nitrogenase reactivity with P-cluster variants. *Proc. Natl. Acad. Sci. USA* **2005**, *102*, 13825–13830. [[CrossRef](#)] [[PubMed](#)]
78. Seefeldt, L.C.; Hoffman, B.M.; Dean, D.R. Mechanism of Mo-Dependent Nitrogenase. *Annu. Rev. Biochem.* **2009**, *78*, 701–722. [[CrossRef](#)] [[PubMed](#)]
79. Danyal, K.; Dean, D.R.; Hoffman, B.M.; Seefeldt, L.C. Electron transfer within nitrogenase: Evidence for a deficit-spending mechanism. *Biochem.* **2011**, *50*, 9255–9263. [[CrossRef](#)]
80. Musgrave, K.B.; Liu, H.I.; Ma, L.; Burgess, B.K.; Watt, G.; Hedman, B.; Hodgson, K.O. EXAFS studies on the  $\text{P}^{\text{N}}$  and  $\text{P}^{\text{OX}}$  states of the P-clusters in nitrogenase. *J. Biol. Inorg. Chem.* **1988**, *3*, 344–352. [[CrossRef](#)]
81. Chan, M.K.; Kim, J.; Rees, D.C. The Nitrogenase FeMo-coand P-cluster pair: A resolution structures. *Science* **1993**, *260*, 792–794. [[CrossRef](#)]
82. Challen, P.R.; Koo, S.K.; Dunham, W.R.; Coucouvanis, D. New  $\text{P}_2\text{-S}_2$ —Coupled, Singly Bridged Double Cubane with the  $[(\text{Fe}_4\text{S}_4\text{C}_{13})_2\text{S}]^{4-}$  Core. *J. Am. Chem. Soc.* **1990**, *112*, 2455–2456. [[CrossRef](#)]
83. Pierik, A.J.; Wassink, H.; Haaker, H.; Hagen, W.R. Redox properties and EPR spectroscopy of the P clusters of *Azotobacter vinelandii* MoFe-protein. *Eur. J. Biochem.* **1993**, *212*, 51–61. [[CrossRef](#)]
84. Kurts, D.M.; McMillan, R.S.; Burgess, B.K.; Mortenson, L.E.; Holm, R.H. Identification of ferritin-sulfur centers in the ferritin-molybdenum proteins of nitrogenase. *Proc. Natl. Acad. Sci. USA* **1979**, *76*, 4986–4989. [[CrossRef](#)]
85. Osterloh, F.; Sanakis, Y.; Staples, R.J.; Münck, E.; Holm, R.H. A Molybdenum-Ferritin-Sulfur Cluster Containing Structural Elements Relevant to the P-Cluster of Nitrogenase. *Angew. Chem. Int. Ed.* **1999**, *38*, 2066–2070. [[CrossRef](#)]
86. Osterloh, F.; Achim, C.; Holm, R.H. Molybdenum-Ferritin-Sulfur Clusters of Nuclearities Eight and Sixteen, Including a Topological Analogue of the P-Cluster of Nitrogenase. *Inorg. Chem.* **2001**, *40*, 224–232. [[CrossRef](#)] [[PubMed](#)]
87. Ohki, Y.; Tatsumi, K. New Synthetic Routes to Metal-Sulfur Clusters Relevant to the Nitrogenase Metallo-Clusters, *Z. Anorg. Allg. Chem.* **2013**, *639*, 1340–1349. [[CrossRef](#)]
88. Eady, R.R. Structure–Function Relationships of Alternative Nitrogenases. *Chem. Rev.* **1996**, *96*, 3013–3030. [[CrossRef](#)] [[PubMed](#)]
89. Kim, J.S.; Rees, D.C. Structural models for the metal centers in the nitrogenase molybdenum-iron protein. *Science* **1992**, *257*, 1677–1682. [[CrossRef](#)]
90. Spatzal, T.; Aksoyoglu, M.; Zhang, L.M.; Andrade, S.L.A.; Schleicher, E.; Weber, S.; Rees, D.C.; Einsle, O. Evidence for Interstitial Carbon in Nitrogenase FeMo Cofactor. *Science* **2011**, *334*, 940. [[CrossRef](#)]

91. Rittle, J.; Peters, J.C. Fe–N<sub>2</sub>/CO complexes that model a possible role for the interstitial C atom of FeMo-co(FeMoco). *Proc. Natl. Acad. Sci. USA* **2013**, *110*, 15898–15903. [[CrossRef](#)]
92. Christiansen, J.; Cash, V.L.; Seefeldt, L.C.; Dean, D.R. Isolation and Characterisation of Acetylene-resistant Nitrogenase. *J. Bio. Chem.* **2000**, *275*, 11459–11464. [[CrossRef](#)]
93. Djurdjevic, I.; Einsle, O.; Decamps, L. Nitrogenase Cofactor: Inspiration for Model Chemistry. *Chem. Asian J.* **2017**, *12*, 1447–1455. [[CrossRef](#)]
94. Holm, R.H.; Lo, W. Structural Conversions of Synthetic and Protein-Bound Ferritin-Sulfur Clusters. *Chem. Rev.* **2016**, *116*, 13685–13713. [[CrossRef](#)]
95. Shah, V.K.; Brill, W.J. Isolation of an ferritin-molybdenum cofactor from nitrogenase. *Proc. Natl. Acad. Sci. USA* **1977**, *74*, 3249–3253. [[CrossRef](#)]
96. Wolff, T.E.; Power, P.P.; Frankel, R.B.; Holm, R.H. Synthesis and Electronic and Redox Properties of “Double-Cubane” Cluster Complexes Containing MoFe<sub>3</sub>S<sub>4</sub> and WFe<sub>3</sub>S<sub>4</sub> Cores. *J. Am. Chem. Soc.* **1980**, *102*, 4694–4703. [[CrossRef](#)]
97. Lancaster, K.M.; Roemelt, M.; Ettenhuber, P.; Hu, Y.; Ribbe, M.W.; Neese, F.; Bergmann, U.; DeBeer, S. X-ray Emission Spectroscopy Evidences a Central Carbon in the nitrogenase Ferritin-Molybdenum Cofactor. *Science* **2011**, *334*, 974–977. [[CrossRef](#)] [[PubMed](#)]
98. Spatzal, T.; Perez, K.A.; Einsle, O.; Howard, J.B.; Rees, D.C. Ligand binding to the FeMo-cofactor: Structures of CO-bound and reactivated nitrogenase. *Science* **2014**, *345*, 1620. [[CrossRef](#)] [[PubMed](#)]
99. Wolff, T.E.; Berg, J.M.; Hodgson, K.O.; Frankel, R.B.; Holm, R.H. Synthetic Approaches to the Molybdenum Site in Nitrogenase. Preparation and Structural Properties of the Molybdenum-Ferritin-Sulfur “Double-Cubane” Cluster Complexes [Mo<sub>2</sub>(SC<sub>2</sub>H<sub>5</sub>)<sub>3</sub>]- and [Mo<sub>2</sub>Fe<sub>6</sub>S<sub>9</sub>(SC<sub>2</sub>H<sub>5</sub>)<sub>8</sub>]<sup>3-</sup>. *J. Am. Chem. Soc.* **1979**, *101*, 4140–4150.
100. Demadis, K.D.; Campana, C.F.; Coucouvanis, D. Synthesis Structural Characterization of the New Mo<sub>2</sub>Fe<sub>6</sub>S<sub>8</sub>(PR<sub>3</sub>)<sub>6</sub>(CL<sub>4</sub>-cat)<sub>2</sub> Clusters. *J. Am. Chem. Soc.* **1995**, *117*, 7832–7833. [[CrossRef](#)]
101. Zhang, Y.; Holm, R.H. Synthesis of a Molecular Mo<sub>2</sub>Fe<sub>6</sub>S<sub>9</sub> Cluster with the Topology of the PN Cluster of Nitrogenase by Rearrangement of an Edge-Bridged Mo<sub>2</sub>Fe<sub>6</sub>S<sub>8</sub> Double Cubane. *J. Am. Chem. Soc.* **2003**, *125*, 3910–3920. [[CrossRef](#)] [[PubMed](#)]
102. Luo, Y.; Li, Y.; Yu, H.; Zhao, J.F.; Chen, Y.H.; Hou, Z.M.; Qu, J.P. DFT Studies on the Reduction of Dinitrogen to Ammonia by a Thiolate-Bridged Diferritin Complex as a Nitrogenase Mimic. *Organometallics* **2012**, *31*, 335–344. [[CrossRef](#)]
103. Li, Y.; Li, Y.; Wang, B.M.; Luo, Y.; Yang, D.W.; Tong, P.; Zhao, J.F.; Luo, L.; Zhou, Y.H.; Chen, S.; et al. Ammonia formation by a thiolate-bridged diferritin amide complex as a nitrogenase mimic. *Nat. Chem.* **2013**, *5*, 320–326. [[CrossRef](#)]
104. Dance, I. Mimicking Nitrogenase. *Dalton Trans.* **2010**, *39*, 2972–2983. [[CrossRef](#)]
105. Leigh, G.J. *Nitrogen Fixation at the Millennium*; Leigh, G.J., Ed.; Elsevier: Amsterdam, The Netherlands, 2003; pp. 299–322.
106. Demadis, K.D.; Malinak, S.M.; Coucouvanis, D. Catalytic Reduction of Hydrazine to Ammonia with MoFe<sub>3</sub>S<sub>4</sub>–Polycarboxylate Clusters. Possible Relevance Regarding the Function of the Molybdenum-Coord—inated Homocitrate in Nitrogenase. *Inorg. Chem.* **1996**, *35*, 4038–4046. [[CrossRef](#)]
107. Malinak, S.M.; Demadis, K.D.; Coucouvanis, D. Catalytic Reduction of Hydrazine to Ammonia by the VFe<sub>3</sub>S<sub>4</sub> Cubanes. Further Evidence for the Direct Involvement of the Heterometal in the Reduction of Nitrogenase Substrates and Possible Relevance to the Vanadium Nitrogenases. *J. Am. Chem. Soc.* **1995**, *117*, 3126–3133. [[CrossRef](#)]
108. McEvoy, J.P.; Brudvig, G.W. Water-splitting chemistry of photo system II. *Chem. Rev.* **2006**, *106*, 4455–4483. [[CrossRef](#)] [[PubMed](#)]
109. Ma, X.; Liu, J.; Xiao, H.; Li, J. Surface cluster catalyst for N<sub>2</sub>-to-NH<sub>3</sub> thermal conversion. *J. Am. Chem. Soc.* **2018**, *140*, 46–49. [[CrossRef](#)] [[PubMed](#)]
110. Roger, I.; Shipman, M.A.; Symes, M.D. Earth-abundant catalysts for electrochemical and photoelectrochemical water splitting. *Nat. Rev. Chem.* **2017**, *1*, 1–10. [[CrossRef](#)]
111. Li, H.; Li, J.; Ai, Z.H.; Jia, F.L.; Zhang, L.Z. Oxygen Vacancy—Mediated Photocatalysis of BiOCl: Reactivity, Selectivity, and Perspectives. *Angew. Chem.* **2018**, *57*, 122–138. [[CrossRef](#)] [[PubMed](#)]
112. Yang, J. Progress of metal oxide(sulfide)-based photocatalytic materials for reducing nitrogen to ammonia. *J. Chem.* **2018**, *2018*, 1–8. [[CrossRef](#)]

113. Thacker, C.M.; Folkins, H.O.; Miller, E.L. Free Energies of Formation of Gaseous Hydrocarbons and Related Substances. *Ind. Eng. Chem.* **1941**, *33*, 584–590. [[CrossRef](#)]
114. Brown, K.A.; Harris, D.F.; Wilker, M.B. Light-driven dinitrogen reduction catalyzed by a CdS: Nitrogenase MoFe-protein biohybrid. *Science* **2016**, *352*, 448–450. [[CrossRef](#)]
115. Liu, J.; Kelley, M.S.; Wu, W.Q.; Banerjee, A.; Douvalis, A.P.; Wu, J.S.; Zhang, Y.B.; Schatz, G.C.; Kanatzidis, M.G. Nitrogenase-mimic ferritin-containing chalcogels for photochemical reduction of dinitrogen to ammonia. *Proc. Natl. Acad. Sci. USA* **2016**, *113*, 5530–5535. [[CrossRef](#)]
116. Banerjee, A.; Yuhas, B.D.; Margulies, E.A.; Zhang, Y.; Shim, Y.; Wasielewski, M.R.; Kanatzidis, M.G. Photochemical nitrogen conversion to ammonia in ambient conditions with FeMoS-chalcogels. *J. Am. Chem. Soc.* **2015**, *137*, 2030–2034. [[CrossRef](#)]
117. Xu, G.; Wang, Z.; Ling, R.; Zhou, J.; Chen, X.D.; Holm, R.H. Ligand metathesis as rational strategy for the synthesis of cubane-type heteroleptic ferritin–sulfur clusters relevant to the FeMo cofactor. *Proc. Natl. Acad. Sci. USA* **2018**, *115*, 5089–5092. [[CrossRef](#)] [[PubMed](#)]
118. Zheng, B.; Chen, X.D.; Zheng, S.L.; Holm, R.H. Selenium as a structural surrogate of sulfur: Template-assisted assembly of five types of tungsten-ferritin-sulfur/selenium clusters and the structural fate of chalcogenide reactants. *J. Am. Chem. Soc.* **2012**, *134*, 6479–6490. [[CrossRef](#)] [[PubMed](#)]
119. DeRosha, D.E.; Holland, P.L. Incorporating light atoms into synthetic analogues of FeMoco. *Proc. Natl. Acad. Sci. USA* **2018**, *115*, 5054–5056. [[CrossRef](#)] [[PubMed](#)]



© 2019 by the author. Licensee MDPI, Basel, Switzerland. This article is an open access article distributed under the terms and conditions of the Creative Commons Attribution (CC BY) license (<http://creativecommons.org/licenses/by/4.0/>).